This is an *Accepted Manuscript*, which has been through the Royal Society of Chemistry peer review process and has been accepted for publication. The final version has been published in *J. Mater. Chem. C, 2017,5, 3509-3518* with doi: https://doi.org/10.1039/C7TC00800G

Double layer capacitance of ionic liquids for electrolyte gating of ZnO thin film transistors and effect of gate electrode.

M. Singh[a], K.Manoli[a], A. Tiwari[a], T. Ligonzo[b], C. Di Franco[c], N. Cioffi[a,d], G. Palazzo[a,d], G. Scamarcio[b,c], L. Torsi[a,d]

Electrolyte gated thin film transistors (TFTs) based on sol-gel processed zinc oxide (ZnO) are investigated using imidazolium-based ionic liquids (ILs), namely [bmim][BF_4], and [bmim][PF_6], as electrolytes. The capacitance of the ILs is determined by means of electrochemical impedance spectroscopy. The frequency dependence of the capacitance measurements indicates that the electric-double-layers (EDLs) form below 1 KHz. Impedance measurements are also acquired at different gate voltages and the effect of the bias is discussed in detail. The experimental data suggest that the double layer capacitance of the two ILs depends on the polarization voltage. In terms of transistor characteristics, minimum hysteresis is observed in the case of the [bmim][BF_4]. Being the smaller out of the two in size, a higher ionic mobility is expected. Therefore, a faster formation of the EDL can account for a suppressed hysteresis in the I-V characteristics. The estimated capacitance was 1.17 μF/cm^2 for [bmim][PF_6] and 4.05 μF/cm^2 for [bmim][BF_4], that resulted in TFT field effect mobility as high as 6.0 and 1.4 cm^2/Vs, respectively. Also the on-off ratio of the EG-TFT is particularly high, being 10^4. Moreover, transient current measurements showed that the two ILs liquid behave differently under continuous bias stress. The role of the metal gate electrode on the device characteristics is also investigated. Five metals of varying work function are employed for establishing the gate/IL interface. The data does not support that there is a correlation between the threshold voltage and the work function of the metals. On the other hand, the capacitance seems to be more susceptible to changes of the metal gate.

Introduction

Over the few last years, thin-film transistors (TFT) based on semiconductor metal oxides have gain considerable interest due to their high charge-carrier mobility, transparency and excellent chemical and mechanical stability.[1-3] Among other, metal oxides semiconductors are potential candidates for transparent electronics as they have excellent electrical properties and at the same time are transparent in the visible region of spectrum.[3] Furthermore, they represent a promising alternative to the amorphous Si based TFTs.[4] Several zinc-oxide (ZnO)[5] derivatives such as indium-zinc-oxide (IZO),[6] indium-gallium-zinc-oxide (IGZO),[7] have been successfully employed as channel layers in TFT devices. In particular, ZnO (a II-VI binary compound) has a wide band gap (3.37 eV), it is non-toxic, highly abundant in nature and can be solution processed.[8-10] Due to its wide band gap, the electronic/optoelectronic devices based on ZnO exhibit some appealing features such as minimum electronic noise, ability to maintain high breakdown voltages and operate at high power. ZnO presents some other favorable properties, such as near UV emission and transparency in visible region, piezoelectricity, pyroelectricity and biocompatibility.[11] Furthermore, the growth of the ZnO thin film through solution-processable methods, like sol-gel processes, renders it compatible with flexible substrates.[12, 13] In this respect particularly interesting is also the use of low-cost processed TFTs for sensing applications.[14, 15]

In the past few years, a new TFT architecture, known as electrolyte-gated TFT (EG-TFT)[16, 17] emerged and has gather significant attention due the possibility to drive the TFT at low voltages. In these devices, an electrolyte serves as a gate medium and, upon application of the gate voltage, EDLs are formed at the gate-electrolyte and electrolyte-semiconductor interfaces. These built-in EDLs are associated with high capacitance values.[16-18] EG-TFT configuration removes the technologically demanding fabrication of ultra-thin dielectric layers and in the case of bioelectronic applications, gives the possibility to gate the device directly through a biological electrolyte solution.[19, 20] In n-type EG-TFT devices, when a positive gate bias is applied *vs.* the grounded source, anions migrate towards the gate-electrolyte interface while the cations gather at the semiconductor-electrolyte interface, leaving a charge-neutral electrolyte in between. This ionic migration leads to a negative charge accumulation at the gate-electrolyte and positive charges at the semiconductor-electrolyte interfaces generating two Helmholtz electrical double layers (HDLs) one at each interface where most of the applied voltage is dropped.[21] The total capacitance of the electrolyte gating layer is determined by the capacitance of the two EDLs connected in series and will never be larger than the smaller of the two single EDLs. The overall value of capacitance can reach several tens of μF/cm^2, thus making it possible to induce a very large charge carrier concentration (~ 10^{15} cm^{-2}) in the transistor channel at low applied gate voltages.[19] Any additional low capacitance layer, such as for instance an oxide layer attached to the gate, being in series with the larger EDLs capacitance, will dominate the total TFT gating capacitance, C_i, and will cause a net drop in the TFT output current.

Solution processed ZnO in form of thin-films or nano-rods have been successfully used as active layers in a number of different electrolyte gated TFTs.[22-24] Furthermore, ZnO-based TFTs gated

Please do not adjust margins

via an ionic conducting poly-4-vinylphenol, have been proposed for all-electrical measurements of a metal work function.[25] The main advantage over organic semiconductors is the higher field-effect mobility and relatively higher stability of ZnO.

Lately, room temperature ionic liquids are being investigated to replace traditional electrolyte solutions so as to reduce solvent evaporation and improve the performance and the stability of EG-TFTs.[18, 26] ILs are organic salts composed of an organic cation and an organic or inorganic anion and exist in liquid state at room temperature. These molten salts, featuring low melting temperature, low vapor pressure, high thermal stability, high ionic conductivity and a large electrochemical stability-window, are considered promising alternatives to gate a TFT.[27] Among others, they are compatible with biological elements, especially enzymes like lipase.[28, 29] Therefore, ILs are appealing for electronic biosensing application.[30] For instance, Yang *et al*.[31] developed an IL gated organic transistor based glucose sensor.

In the present contribution, we study a solution-processed ZnO EG-TFT gated through two ionic liquids, that are 1-Butyl-3-methylimidazolium hexafluorophosphate, [bmim][PF_6], and 1-Butyl-3-methylimidazolium tetrafluoroborate, [bmim][BF_4]. Electrochemical impedance spectroscopy (EIS) measurements were carried out to study the capacitive behavior of the two ILs in contact with the ZnO semiconductor surface. The impedance data are acquired at different gate voltages and the effect of the bias voltage on the overall capacitance is investigated. In addition, a systematic study on the effect of tungsten (W), nickel (Ni), platinum (Pt), palladium (Pd), and gold (Au) gates work function (ϕ) onto the ILs- gated ZnO TFT performance is presented. Finally, the operational stability of the ILs gated ZnO TFT under constant drain-source and gate voltage is presented.

Experimental

Ionic liquids, [bmim][PF_6], [bmim][BF_4] were purchased from Sigma-Aldrich and used without any further treatment. The selected ILs share the same cation but differ in the anion. Their chemical structure is illustrated in Figure 1. ZnO was prepared using the sol-gel method. For the precursor solution, zinc acetate dihydrate, ($Zn(CH_3COO)_2 \cdot 2H_2O$, 99,9%, Sigma Aldrich) was dissolved in ethanol with a final concentration of 0.1 M. The solution was stirred for 7 hours at 70 ^{0}C, until a transparent, homogenous solution was obtained.

For the EG-TFT fabrication, Au / Ti (50 nm/ 5 nm) source (S) and drain (D) interdigitated electrodes defined the TFT channel with a length L = 10 µm and 2µm and width (W) of 1mm. The electrodes with 10 µm channel length were fabricated with photolithography, while for the smaller ones (L= 2 µm) e-beam lithography was employed. The e-beam lithography was performed using Raith system. The patterned Si/SiO_2 substrates were cleaned with piranha solution (3:1 mixture of sulfuric acid and hydrogen peroxide). Afterwards, they were thoroughly rinsed with solvents of increasing polarity (*i.e.* acetone, isopropyl alcohol and deionized water). The precursor solution was deposited on the S–D patterned substrates by spin coating. The thin-film deposition was performed by dispensing 70 - 80 µL droplet of precursor solution on the substrate and subsequent spinning at 2000 RPM for 60 seconds. A film thickness of 46 ± 5 nm was obtained by repeating the precursor deposition procedure three times.[24] After each coating, the deposit was pre-heated at 150 ^{0}C for 10 min to remove any organic residue. Finally, the film was calcined at 393 ± 2^{0}C for 5 hours on a hot plate in air. The TFT structure is shown in Figure 2.

For the impedance measurements, a sandwich like structure involving both the ZnO and the IL was used. This configuration was employed since it resembles the EG-TFT structure. In particular, the samples were prepared as following. A bottom gold electrode, with a surface area of 0.09 cm^2, was lithographically patterned and deposited via e-beam evaporation onto a Si/SiO_2 substrate. On that, the ZnO film was deposited as previously described. Each IL was drop casted on the ZnO surface and a second gold electrode was placed on the top (Figure 2).

Impedance measurements were performed with an Alpha high-resolution dielectric analyzer (Novacontrol GmbH). The impedance (Z) spectra were recorded in the 0.01 Hz to 1 MHz frequency range by applying a V_{AC} = 50mV sine-wave voltage signal perturbation. A DC voltage of 0.0 V and -1.5 V was superposed to the AC signal. The data were plotted as imaginary

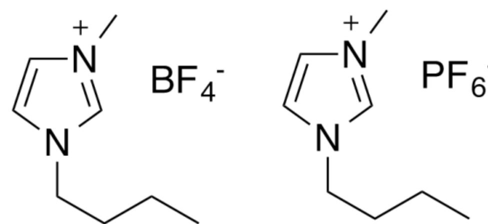

Figure 1: Chemical structures of [bmim][BF_4] (left) and [bmim][PF_6] (right)

vs. real part (-ImZ vs. ReZ) (Nyquist plot) and fitted with suitable software (EIS Spectrum analyzer) able to model an equivalent electrical circuit.

The phase angle (ϑ) and capacitance (C) are calculated according to:

$$\vartheta = arctan\left(\frac{Z''}{Z'}\right), \quad C = \frac{Z''}{\omega(Z'^2 + Z''^2)} \qquad (1)$$

where Z', Z'' are the real and imaginary part of impedance respectively, and ω is the angular frequency of the AC signal.

The current – voltage (I-V) characteristics of ILs gated ZnO TFTs were recorded with a Semiconductor Parameter Analyzer (Agilent 4155C). Five different L-shaped metals (*i.e.* W, Ni, Pt, Pd, Au) were employed as gate electrodes. The ZnO - TFTs were characterized by measuring the I_{DS}-V_{DS} output characteristics, where the drain to source current (I_{DS}) is recorded at different gate voltages (V_G) ranging from 0 to 1 V or up to 1.5 V with a step of 0.1V, while the source and drain bias (V_{DS}) is swept from 0 to 1V or till 1.5 V The transfer characteristics (I_{DS} *vs.* V_G) were recorded by keeping V_{DS} constant at 1 V or 1.5V and sweeping the V_G from 0 to 1 or till 1.5V with a step of 0.02V. Furthermore, transient current measurements were recorded for 45 minutes by applying constant V_{DS}= V_G= 1V to investigate the stability of

Please do not adjust margins

Please do not adjust margins

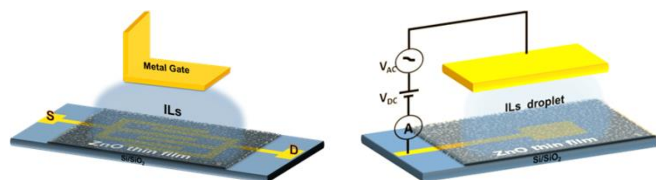

Figure 2: ZnO TFT structure (on the right), Au/ZnO/IL/Au structure used for EIS measurements (on the left)

the devices. All electrical measurements were carried out in ambient air at relative humidity of 35±5% and at T= 17 - 20 °C. Field effect mobility (μ), threshold voltage (V_T) and the on/off current ratio (I_{ON}/I_{OFF}) were extracted from the transfer characteristic curves in the saturation regime. In this regime the drain current is given by[32]:

$$I_{DS} = \frac{W}{2L}\mu * C_i(V_G - V_T)^2 \qquad (2)$$

where C_i is the capacitance per unit area. According to equation 2, the square root of the I_{DS} is equal to:

$$\sqrt{I_{DS}} = \left(\frac{W}{2L}\mu * C_i\right)^{\frac{1}{2}} V_G - \left(\frac{W}{2L}\mu * C_i\right)^{\frac{1}{2}} V_T \qquad (3)$$

In particular, μ and V_T were defined graphically from the plot of ($|I_{DS}|^{1/2}$) *vs.* V_G, based on equations 4 and 5, respectively.

$$\mu = \frac{B^2 2L}{WC_i} \qquad (4)$$

$$V_T = -\frac{A}{B} \qquad (5)$$

where $B = \left(\frac{W}{2L}\mu * C_i\right)^{\frac{1}{2}}$ is the slope of the linear part of the graph and A= -B*VT the intercept.

The I_{ON}/I_{OFF} was determined by taking the value of I_{ON} at V_{DS} = V_G = max and I_{OFF} at V_{DS} = max and V_G = 0V.
Cyclic voltammetry in neat ILs interfaced with different metal electrodes was used to assess any electrochemical processes within the potential window that matches the gate voltage applied during the TFT measurements (*i.e.* from -0.1 V to 1 V, scan rate 50 mV/sec). The different gate metals were employed as working electrodes (WE). All metals held the same surface area and before measuring they were polished with aluminum oxide powder, followed by rinsing with HPLC water and kept in an ultra-sounds bath of isopropanol for 30 min. The counter electrode (CE) and the reference electrode (RE) were made of Au. A sufficiently smaller surface area of the WE with respect to that of the CE was kept. All potentials are reported against Au as RE.

Results and discussion

Measurement of the electrical double layer capacitance

The capacitance of EDL in ILs depends on many variables including electrode potential, temperature, ionic concentrations, types of ions, oxide layers, electrode roughness, impurity adsorption, *etc*.[18] According to *eq*. 4, the calculated field effect mobilities depend on the capacitance of the gating medium. Therefore, any uncertainty assigned to capacitance affects the mobility. To derive more accurately the mobility in the electrolyte gated ZnO-TFTs and understand the charge polarization dynamics within each IL droplet, we first have to measure the capacitance of the EDL formed at the two interfaces of the IL with the ZnO and the Au metal gate. We performed electrochemical impedance spectroscopy measurements for Au/ZnO/[bmim][PF_6]/Au and Au/ZnO/[bmim][BF_4]/Au capacitor like structures.
Figures 3a and 3b show the impedance phase angle as a function of the frequency, as obtained at 0 V and -1.5 V DC bias. The phase behavior of the impedance spectra allows discriminating if the system yields a resistive or a capacitive character. In the absence of a DC bias, the phase angle is around - 80° at low frequencies for both systems. This is indicative of a capacitive behavior and the formation of the EDLs at the interfaces. While in the high frequency region (>10 KHz), the phase angle is small ($-45° < \theta < 0°$), corresponding to a resistive behavior.[18] When a DC bias is applied, we find that the phase angle reaches a maximum at around 1KHz, and the curves become more symmetrical versus the log(*f*). Yuan *et al.*,[33] attributed the voltage dependent behaviour of the phase

Please do not adjust margins

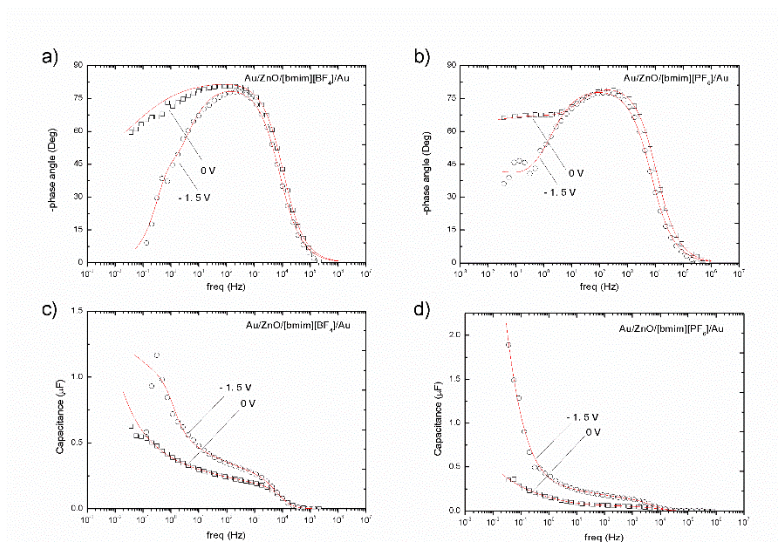

Figure 3: Impedance phase angle vs. frequency for a) Au/ZnO/[bmim][BF_4]/Au and b) Au/ZnO/[bmim][PF_6]. Capacitance vs. frequency for c) Au/ZnO/[bmim][BF_4]/Au and b) Au/ZnO/[bmim][PF_6].Solid line is fitted based on the equivalent circuits reported in Figure 6.

angle and of the impedance to bias induced leak current passing through the EDL interface.

The frequency profile of the capacitance in the two systems is shown in Figures 3c and 3d. The capacitance value is small in high frequencies, while it increases with decreasing the frequency. In the high frequency region (> 10 KHz), capacitance tends to attain a constant value which corresponds to the geometric capacitance with the IL acting as dielectric. In this region, the capacitance is dominated by the bulk IL capacitance. By decreasing the frequency, the ions start following the applied AC signal and their migration results into the formation of Helmholtz layers along the ZnO and Au electrode surface. When the frequency decreases less than 1Hz, an accelerating increase in capacitance is observed in all cases. More intense is the increase upon the DC bias, leading to a capacitance of few tens of $\mu F/cm^2$ for both ILs.

Variations of the capacitance with applied bias depend on the shape, size and chemical structure of the electrolyte ions.[18] In order to investigate the influence of the polarization potential on the dielectric properties of the two systems, capacitance versus potential curves were obtained at a constant frequency (20Hz) for [bmim][PF_6] and [bmim][BF_4] as shown in Figure 4. The capacitance is fairly stable for both ILs upon positive bias, whereas it increases as we move to negative voltages. In the case of the bigger sized anion ([bmim][PF_6]), the value of the capacitance seems to depend slightly on the voltage from +2 V down to zero dc bias. Between 0 and -1V it increases, to reach a second higher plateau below -1V. The value of capacitance is almost four times higher than that at zero bias. For the smaller sized anion ([bmim][BF_4]), saturation is not clearly reached, at least down to -2V. In terms of comparison, the EDL capacitance for [bmim][BF_4] is larger than [bmim][PF_6] at 20 Hz. For a fixed cation, the capacitance increases as the anion size decreases, since smaller and less sterically demanding ions can lead to more densely packed EDLs. Such an order is consistent with previously reported studies.[34, 35] In addition, [bmim][BF_6] is characterized by lower ion mobility than [bmim][BF_4].[26] Larger, less mobile anions can cause a drop in ionic conductivity and capacitance compare to smaller sized ions.

Electrical equivalent circuit modeling

The complex impedance can be expressed as the sum of its real, Z', and imaginary, Z", parts. The Nyquist plots (-Z" vs. Z') for

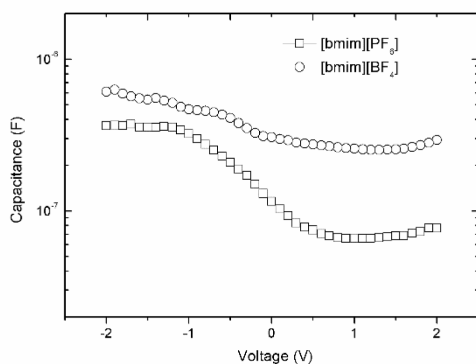

Figure 4: Capacitance vs. voltage at constant frequency (f = 20Hz) for Au/ZnO/[bmim][PF_6]/Au and Au/ZnO/[bmim][BF_4]/Au.

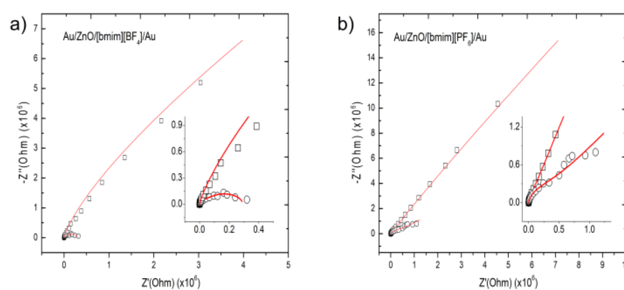

Figure 5: Nyquist plot of impedance spectra for a)Au/ZnO/[bmim][PF_4]/Au and b) Au/ZnO/[bmim][BF_6]/Au at at V_{DC} = 0 V (square) and V_{DC} = -1.5V (circle) with magnified inset. The solid lines are fitted based on the equivalent circuits reported in Figure 6.

Please do not adjust margins

[bmim][BF_4] and [bmim][PF_6] are similar by shape, but strongly depend on the polarization potential (Figure 5). The impedance spectra of both ILs show a straight line with a slight

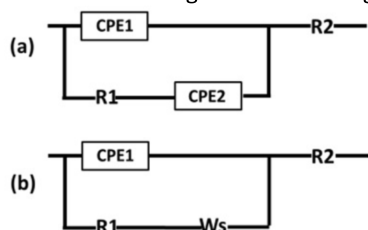

Figure 6: Equivalent circuits of Au/ZnO/IL/Au at (a) V_{DC} = 0 V and (b) V_{DC} = -1.5V

curvature in the absence of DC bias. Assuming that no Faradaic reactions occur at the electrode surface, a Nyquist plot of the impedance spectrum in ionic liquids is a straight line with a slight curvature at low frequencies. The measurements confirm that a capacitor effect is dominating, while the tilt of the lines indicates a small contribution of the resistive components. This corresponds to a typical electrolyte behavior. [36] Application of gate bias has a large effect on the impedance. Impedance is greatly decreasing and the Nyquist plots bend downwards, resembling semicircles (inset of Fig. 5).

The impedance spectra could be represented by a three-element electrical equivalent circuit, including a constant phase element (CPE), a resistor R and the Warburg element (W). Herein, two different equivalent circuit models are employed to describe the data. The first equivalent circuit model (Figure 6a) is used to represent the impedance data that were collected at zero dc bias voltage. In this model, the CPE1 represents the actual EDL capacitance. CPE1 is in parallelwith a branch containing (in series) the bulk ionic liquid resistance (R1) and CPE2. This whole combination is further in series with the contact resistance (R2). CPE2 is essentially a Warburg resistance, representing the contribution of ion diffusion taking place in an infinite region due to the formation of inhomogeneous EDL. The second equivalent circuit model (Figure 6b) represents the impedance data that were collected at -1.5V dc bias. In this model, the CPE1 is again the EDL capacitance and it's in parallel with a branch containing (in series) R1 and Warburg short (Ws). The combination of these elements is in series with R2. The Warburg short (Ws) represents the impedance of finite-length diffusion with transmissive boundaries that occurs when the dc bias of -1.5V is applied and a uniform EDL is formed.[37] Further details are given in the supplementary information (SI).

Based on these two equivalent circuits, the impedance data were fitted using the EIS spectrum analyzer software *[http://www.abc.chemistry.bsu.by/vi/analyser]*.[38] Parameters such as R1, CPE, n *etc.* were determined and are presented in Table S1 (SI).

Imposing that $Z_{CPE1} = 1/Q(j\omega)^n = 1/j\omega C$ (see SI). The electric double layer capacitance (C_{EDL}) can be derived from:

$$C_{EDL} = Q\,\omega^{n-1} \qquad (6)$$

where $\omega = 6.28\times10^{-1}$ rad/s at $f = 10^{-1}$ Hz.

The values of the capacitance for [bmim][BF_4] and [bmim][PF_6] at 0 and -1.5 V dc bias are presented in Table 1. The capacitance is strongly dependent from the polarization potential. The double layer capacitance increases upon dc bias This suggests that more homogenous and compact EDLs are formed when a dc bias is applied. The smaller anion based IL yields a higher capacitance than the larger one. However, the larger anion seems to undergo greater changes upon bias. A three times higher capacitance is observed, while less than double is the change in the capacitance value for the smaller anion.

Electrical performance of the ILs gated ZnO based TFT

The electrical performance of the EG-TFT was evaluated for transistors gated through [bmim][BF_4] and [bmim][PF_6]. Representative output and transfer characteristics graphs are shown in Figure 7. From the I-V output characteristics we observe that, as the V_{DS} bias is swept, the drain current exhibits well shaped linear and saturation region and also shows good modulation (on/off ratio as high as 3×10^4) (Figures 7a and 7b). Figures 7c and 7d illustrate the I-V transfer characteristic curves with the drain current plotted in logarithmic scale along with the square route of I_{DS} and the resulting fitting in the linear part of the curve. The TFTs gated with both ILs show mutually close drain current. We note that the [bmim][PF_6] gated device exhibits hysteretic behavior, as shown by the mismatching of the forward and reverse voltage sweep.

According to equation 4, mobility depends mainly on two factors, the slope (B) of the linear part of the curve and the value of the relevant capacitance, while W/L ratio is a constant quantity. The experimental values of the slope B, calculated form the sqrt(I_{DS}) *vs*. V_G plots, were found to be 0.06 ± 0.01 and 0.05 ± 0.01 for [bmim][PF_6] and [bmim][BF_4] gating medium, respectively. Thus we can consider them indistinguishable within the experimental uncertainty.

Using the values of EDL capacitance, calculated from the EIS measurements upon 0V and -1.5V bias, the corresponding mobility values have been estimated. Since the slope B is independent form the nature of the IL, the estimated mobility of ZnO depends essentially on the measured EDL capacitance, assuming that the capacitance is equal to the electrical double layer capacitance (*i.e.* $C_i = C_{EDL}$). The calculated value of mobility is 6.0 cm^2/Vs for [bmim][PF_6] and 1.4 cm^2/Vs for [bmim][BF_4]. Similar values for both ILs are found for the threshold voltage and the $I_{ON/OFF}$ ratio. The figures of merit averaged over 5 different devices with the relevant uncertainties are reported in Table 1.

As seen, the hysteresis in case of the transistor gated with [bmim][PF_6] is visibly larger as compared to the TFT gated with [bmim][BF_4]. The drain current is lower in the reverse swept of the drain voltage, suggesting that the number of mobile charges is smaller than in the forward voltage swept. Kergoat *et. al.*[39] suggested that the hysteresis in the TFT characteristics

Please do not adjust margins

Please do not adjust margins

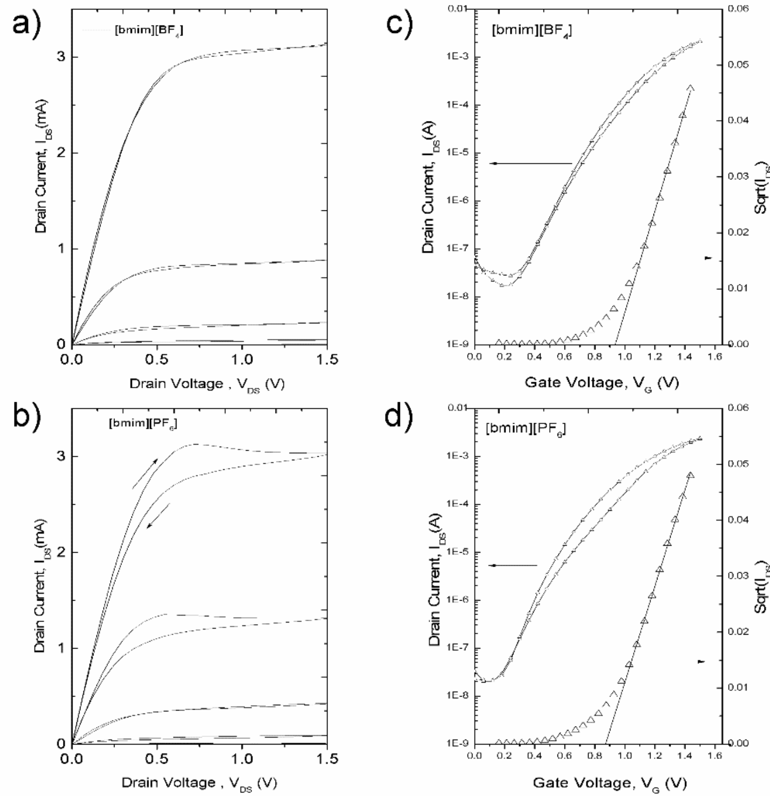

Figure 7: I-V output characteristics of ZnO TFT gated with a) [bmim][BF_4] and b) [bmim][PF_6]. I-V transfer characteristics of ZnO TFT gated with c) [bmim][BF_4] and d) [bmim][PF_6]. The measurements are realized using S-D electrodes with L=10µm, W=10 mm.

Table 1: Capacitance values of ILs and average values of mobility, threshold voltage and I_{ON}/I_{OFF} ratio of the IL gated ZnO TFTs

ILs	C_{EDL} (µF/cm²) 0V	C_{EDL} (µF/cm²) -1.5 V	µ (cm²/Vs) 0V	µ (cm²/Vs) -1.5V	V_T (V)	I_{ON}/I_{OFF}
[bmim][PF_6]	1.17	3.79	6.0±2.62	1.9±0.81	0.84±0.02	2.4×10^4
[bmim][BF_4]	4.05	6.93	1.4±0.82	0.8±0.48	0.90± 0.01	1.8×10^4

can occur due to ion penetration into the bulk of the semiconductor and/or to the rate of formation of the EDL. With respect to the latter point, a fast formation of the EDL gives rise to low hysteresis. Similar type of hysteresis response was also found by De Tullio *et al.*[26] while studying P3HT based TFT gated with [bmim][PF_6] and [bmim][BF_4]. According to the authors, [bmim][BF_4] has higher ionic mobility than [bmim][PF_6]. Hence, in [bmim][BF_4], a faster formation of EDL occurs, giving rise to lower hysteresis in the I-V characteristics. In contrast, low ion mobility results in a larger hysteresis in the devices gated with [bmim][PF_6].

Electrical stability of the TFT devices in ambient environment

One of the important aspects of the TFT devices is their stability when a constant bias is applied. Transient drain current measurements were carried out for both ILs gated ZnO TFTs over a period of 45 min in air and under continuous bias of V_{DS} = V_G = 1V (Figure 8). An increase in the current is observed in the first 1-2 min and it is probably due to the initial rearrangement of the ZnO/IL interface. On a longer timescale, a drift in the current I_{DS} is observed for EG-TFT gated using the two ILs with opposite trend. As the cumulative IL biasing time increases, on-current increases in case of the ZnO TFT gated with [bmim][PF_6]. The opposite is true for the device gated with [bmim][BF_4].

Increase of the drain current upon bias stress of an a-IGZO based TFT gated with 1-hexyl-3-methylimidazolium bis(triflluoromethylsulfonyl)imide [Hmim][TFSI] was also observed by Pudasaini *et al.*[40] It was suggested that the high electric field induced by the EDL formed at the interface between the IL and a-IGZO surface, could be responsible for the creation of oxygen vacancies and consequent migration of oxygen from the oxide into the IL. This process gave rise to the drain current upon time.

On the other hand, the current is decreasing when the device is gated with [bmim][BF_4]. Regardless their miscibility with H_2O, all ionic liquids are hygroscopic and if exposed to air can absorb moisture to some extent. It should be noted that some properties of ionic liquids have been shown to depend strongly

Please do not adjust margins

Please do not adjust margins

on the concentration of impurities and water. For instance,

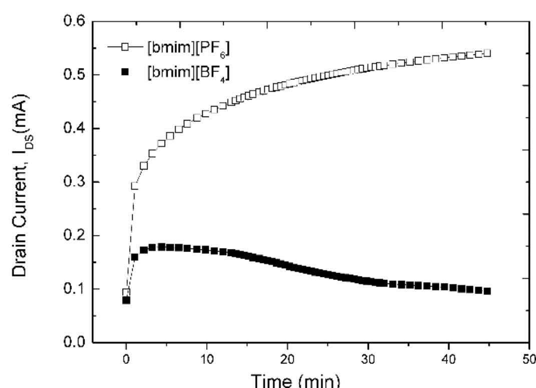

Figure 8 Drain current versus time of the ILs gated ZnO TFTs at constant V_{DS} =V_{GS} = 1V.

water adsorption can significantly change the performance of ILs and affect the stability of the TFTs in ambient air. Therefore, hydrophobic anions are more preferable for such applications. Herein, among the two anions, BF_4 is considered much more hydrophilic than PF_6.[34] Thus, its higher water affinity can be the origin of the device degradation in air.

Effect of metal gate work-function on the performance of IL gated ZnO TFTs

As earlier introduced, the pair of ILs studied in this work, differs solely in the anion. Given that ZnO is n-type material, anions are accumulated at the metal/IL interface upon gate bias. Herein, the transistors performance was assessed with five different metal-gate electrodes; in order to investigate the effect of the metal gate on the performance of the IL gated ZnO TFTs. We should note here that the electrical measurements were performed using the e-beam prepared interdigitated S-D electrodes (L=2µm, W=10 mm). The transfer I-V curves are presented in Figure 9 for all metal gates.

The devices exhibit typical n- type behavior. The transistors with W- and Ni- gates tend to reach higher drain current, few mA, compared to Au-, Pt- and Pd- gates. The drain current decreases from lower to higher work function (ϕ) metal gates. This is true for both ILs. As ZnO conduction band edge lies at 4.3 eV respect to the vacuum level, the tungsten work function (4.48 eV) is the closest. Thus the W-metal gate is expected to have the lowest injection barrier for the electrons. This barrier increases as the work function of gate metal is increased.[41]

In Table 2, the mean values along with the standard deviation of $\mu*C_i$, V_T and the average I_{ON}/I_{OFF} ratio for each of the five gate electrodes used in this study are reported. The work function values for the different gate metals are only indicative as they correspond to measurements realized in high vacuum and can vary depending on a number of factors, such as contamination of the metal surfaces due to the presence of oxides or of a residual water layer.[42] Also, we should note that in case of Ni, the values of the V_T were estimated by the average curve of the forward and reverse sweep due to the observed hysteresis.

In principle, the work function of the gate electrode is more likely to impact on the threshold voltage. Moreover, for n-type ZnO, a positive shift of the V_T is expected with increasing the work function, as the difference between the metal work function and ZnO conduction band increases. In the present case, the measured V_T does not scale with the work function (Figure 10 a). This can be attributed to variations of the actual work function of the metals used in this study with respect to the reported values found in literature (table 2). On the other hand, the product of µ*Ci seems to have a trend with the work function. It decreases with increasing the work function in both ILs.

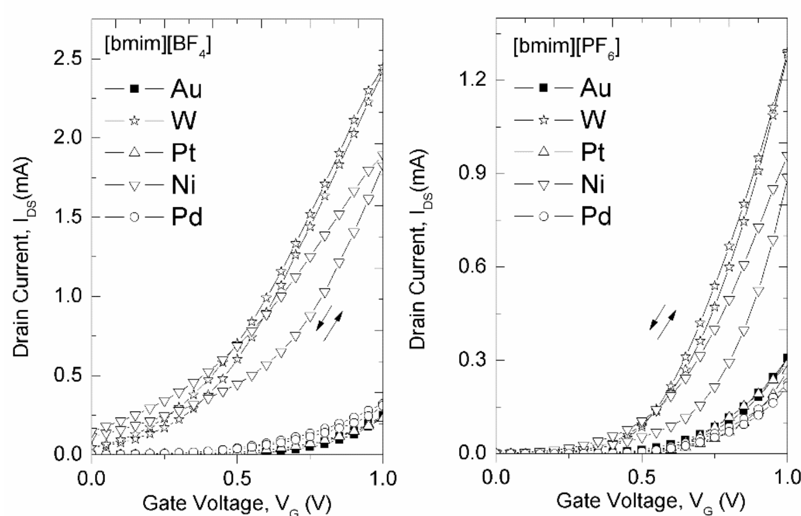

Figure 9: Transfer characteristics of [bmim][BF_4] (left) and [bmim][PF_6] (right) gated ZnO based TFT measured with five different metal gates.

Please do not adjust margins

Table 2: Average values μ*Ci product, VT and I_{ON}/I_{OFF} of ILs gated ZnO -TFT measured with different metal gates.

Gates (ϕ/eV)†	[bmim][BF4]			[bmim][PF6]		
	μ*C_i /F/Vs	V_T /V	I_{ON}/I_{OFF} ratio	μ*C_i /F/Vs)	V_T /V	I_{ON}/I_{OFF}ratio
W (4.48)	(1.2 ± 0.1) × 10^{-6}	0.13± 0.16	10^2	(1.2 ± 0.2) × 10^{-6}	0.30± 0.12	10^3
Ni (5.20)	(8.9 ± 1.8) × 10^{-7}	0.03± 0.10	10	(5.8± 2.1) × 10^{-7}	0.43± 0.07	10^2
Au (5.38)	(4.0 ± 1.2) × 10^{-7}	0.42 ± 0.05	10^3	(3.3±0.4) × 10^{-7}	0.38±0.11	10^3
Pd (5.41)	(2.2 ± 0.3) × 10^{-7}	0.26± 0.01	10^2	(2.6± 0.9) × 10^{-7}	0.31±0.10	10^3
Pt (5.55)	(2.7 ± 0.3) ×10^{-7}	0.40 ± 0.05	10^3	(4.4± 2.2) ×10^{-7}	0.47± 0.06	10^3

†The value of the work function for each metal is the median of the work function range given in [43, 44]

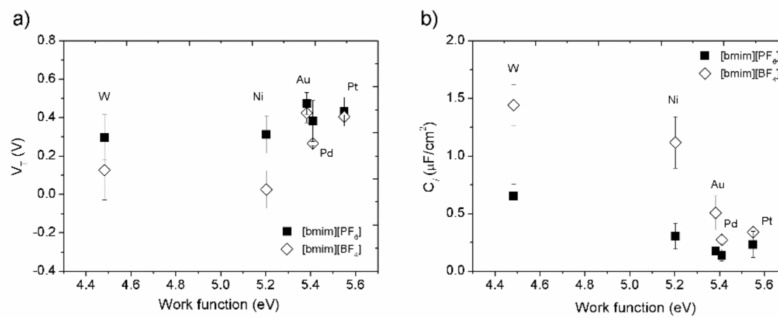

Figure 10: Variation of V_T and C_i for the different metal gate electrodes

To account for the threshold shift, we should consider the following equation which correlates the flat-band voltage (V_{FB})[32] and the work-function difference between the gate material and the semiconductor:

$$V_{FB} = (\phi_m - \phi_s)/q - Q_f/C_i \qquad (7)$$

where ϕ_m and ϕ_s are the metal and the semiconductor work function, Q_f is the fixed charge present at the interface between the semiconductor and the electrolyte, C_i the capacitance per unit area of the gating system and q is the elementary charge. If Q_f is zero, V_{FB} equals V_T, but this refers to an ideal case. In EG-TFTs it is more likely that $Q_f \neq 0$, then the effective gating capacitance, C_i, needs to be considered as well. Therefore, we have estimated the capacitance assuming a constant mobility for ZnO with each IL (*i.e.* 0.8 cm²/Vs for [bmim][BF4] and 1.9 cm²/Vs for [bmim][PF6]). The capacitance values obtained for different metal gates for the devices gated with [bmim][BF4] and [bmim][PF6] are shown in figure 10b. A higher C_i for W and Ni as compared to Au, Pt and Pd is observed. Moreover, the values of capacitance for the metal gates in case of [bmim][BF4] are also larger than [bmim][PF6]. This refers to the same trend as observed for the capacitance values calculated form EIS measurements.

A significant higher capacitance has been seen with water gated ZnO-TFTs using tungsten as the gate electrode.[41] In that case, Ni, Pd, Au and Pt electrodes were electrochemically stable in the potential range that the TFT was operated. On the other hand, and based on the higher leakage current observed, W gate was electrochemically active, leading to an increase of capacitance and consequently to higher current. To address the occurrence of redox processes between the different metal and the ILs, cyclic voltammetry measurements of neat ILs were carried out. The CV of [bmim][PF6] with different metal gates as WE is shown in Figure 11b.

The voltammograms indicate that there is no faradaic current within the potential limits selected for Au, Pt and Pd, whereas for W, Ni electrodes there is some evidence of minimal faradaic current in the anodic potential range.[34, 45] This is also true, but not so profound, if we compare the leakage current (known also as gate current) in [bmim][PF6] gated ZnO-TFTs (Fig. 11a). The leakage current corresponds to the current that flows through the electrolyte in EG-TFTs and although is below 1 μA, we see that W and Ni tend to show higher values than the other three metals.

Commonly, ILs have a potential window of more than 2.0 V, but the presence of water and/or impurities in the ILs can radically reduce the anodic and cathodic potential limits.[46] For instance the electrochemical window of [bmim][BF4] and [bmim][PF6] was found to reduce dramatically (from 4 to 2 V) by adding water.[47] It should be also noted that the potential window is correlated to the electrode material. Besides, under certain conditions, ILs incorporating $[PF_6]^{-1}$ can react with water producing redox active species.[48]

Nevertheless, an increase of the current intensity for the IL in contact with W and Ni, suggests an increase of the double layer capacitance compare to Au, Pt and Pd. [45] This is in agreement

Please do not adjust margins

with the trend of the capacitance observed in the ZnO-TFT devices. Unlike water and conventional organic solvents, the

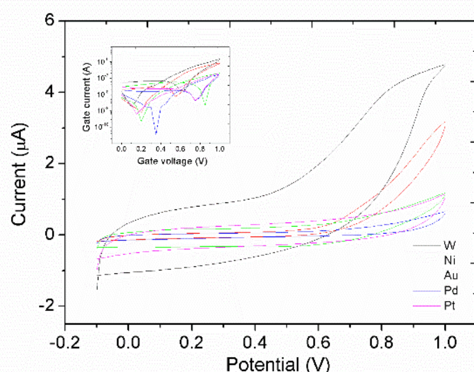

Figure 11: Cyclic voltammetry of neat [bmim][PF_6] on W, Ni, Au, Pd and Pt electrode (scan rate 50 mV/s). Inset: Gate current versus gate voltage for [bmim][PF_6] gated ZnO-TFTs with different gate metals.

capacitance /potential curves have been found to vary significantly with the electrode materials in ILs. Such an effect can be evident by changes in double layer capacitance when the electrode material is altered. If ionic specific adsorption is negligible, such variations have been correlated to the metal work function together with orientation of solvent dipoles in the Helmholtz layer region.[34, 46] To a first approximation, we may assume that the capacitance changes can reflect the changes in work function. These changes can be due to polarization phenomena at the metal/electrolyte interface. Of course the correlation is not so direct and further investigation is needed to be carried out.

Conclusions

In conclusion, we have investigated the performance of solution processed ZnO-TFTs gated through two ILs that differ solely in the anion. The capacitance of each gating system was determined by EIS. Both the capacitance and phase angle variation with frequency indicated the domination of electric double layer (EDL) capacitance in the lower frequency region. While in the higher frequency region, both ILs show a resistive behavior. The capacitance was found to depend greatly on the polarization potential. The double layer capacitance increased upon dc bias, indicating that more homogenous and compact EDLs are formed when a dc bias is applied. Although, a higher capacitance was found for the smaller anion, the capacitance of the larger sized anion showed to undergo greater changes upon DC bias. The performances of the ZnO-TFTs for both ILs were found to be very much alike in terms of current, threshold voltage and mobility. Opposite was the trend of the device upon bias stress measurements, showing an increase of current with time when gated with [bmim][PF_6], while a current degradation was observed in case of [bmim][BF_4]. Finally, significant changes in double layer capacitance of the ILs were observed by altering the gate electrode, whereas there was no clear correlation between the threshold voltage and the work function of the metals.

Acknowledgements

We thank Dr. M. Y. Mulla and Dr. M.Magliulo for useful discussions. Dr. M. V. Santacroce is acknowledged for providing the e-beam S&D interdigitated substrates. The “OrgBIO” Organic Bioelectronics (PITN-GA-2013-607896), the PON SISTEMA (MIUR) projects and CSGI are acknowledged for the financial support.

Notes and references

1 R. A. Street, *Advanced Materials*, 2009, **21**, 2007.
2 G. Adamopoulos, S. Thomas, P. H. Wöbkenberg, D. D. Bradley, M. A. McLachlan and T. D. Anthopoulos, *Advanced Materials*, 2011, **23**, 1894.
3 E. Fortunato, P. Barquinha and R. Martins, *Advanced Materials*, 2012, **24**, 2945.
4 S. J. Kim, S. Yoon and H. J. Kim, *Japanese Journal of Applied Physics*, 2014, **53**, 02BA02.
5 X. Xu, Q. Cui, Y. Jin and X. Guo, *Applied Physics Letters*, 2012, **101**, 222114.
6 K.-B. Park, J.-B. Seon, G. H. Kim, M. Yang, B. Koo, H. J. Kim, M.-K. Ryu and S.-Y. Lee, *IEEE Electron Device Letters*, 2010, **31**, 311.
7 G. H. Kim, B. Du Ahn, H. S. Shin, W. H. Jeong, H. J. Kim and H. J. Kim, *Applied Physics Letters*, 2009, **94**, 233501.
8 B. S. Ong, C. Li, Y. Li, Y. Wu and R. Loutfy, *Journal of the American Chemical Society*, 2007, **129**, 2750.
9 D. C. Look, Materials Science and Engineering: B, 2001, **80**, 383.
10 D. Thomas, Journal of Physics and Chemistry of Solids, 1960, **15**, 86.
11 Ü. Özgür, Y. I. Alivov, C. Liu, A. Teke, M. Reshchikov, S. Doğan, V. Avrutin, S.-J. Cho and H. Morkoc, *Journal of applied physics*, 2005, **98**, 11.
12 E. Luna-Arredondo, A. Maldonado, R. Asomoza, D. Acosta, M. Melendez-Lira and M. d. l. L. Olvera, *Thin solid films*, 2005, **490**, 132.
13 N. R. Farley, C. R. Staddon, L. Zhao, K. W. Edmonds, B. L. Gallagher and D. H. Gregory, *Journal of Materials Chemistry*, 2004, **14**, 1087.
14 F. Marinelli, A. Dell'Aquila, L. Torsi, J. Tey, G. Suranna, P. Mastrorilli, G. Romanazzi, C. Nobile, S. Mhaisalkar and N. Cioffi, *Sensors and Actuators B: Chemical*, 2009, **140**, 445.
15 L. Torsi, F. Marinelli, M. D. Angione, A. Dell'Aquila, N. Cioffi, E. De Giglio and L. Sabbatini, *Organic Electronics*, 2009, **10**, 233.
16 K. Hong, S. H. Kim, K. H. Lee and C. D. Frisbie, *Advanced Materials*, 2013, **25**, 3413.
17 L. Kergoat, L. Herlogsson, D. Braga, B. Piro, M. C. Pham, X. Crispin, M. Berggren and G. Horowitz, *Advanced Materials*, 2010, **22**, 2565.
18 S. Thiemann, S. Sachnov, S. Porscha, P. Wasserscheid and J. Zaumseil, *The Journal of Physical Chemistry C*, 2012, **116**, 13536.
19 E. Said, X. Crispin, L. Herlogsson, S. Elhag, N. D. Robinson and M. Berggren, *Applied Physics Letters*, 2006, **89**, 143507.
20 M. Y. Mulla, E. Tuccori, M. Magliulo, G. Lattanzi, G. Palazzo, K. Persaud and L. Torsi, *Nature communications*, 2015, **6**.
21 K. Manoli, M. Magliulo, M. Y. Mulla, M. Singh, L. Sabbatini, G. Palazzo and L. Torsi, *Angewandte Chemie International Edition*, 2015, **54**, 12562.
22 A. Al Naim and M. Grell, *Applied Physics Letters*, 2012, **101**, 141603.

Please do not adjust margins

Please do not adjust margins

23 S. Thiemann, M. Gruber, I. Lokteva, J. Hirschmann, M. Halik and J. Zaumseil, *ACS applied materials & interfaces*, 2013, **5**, 1656.
24 M. Singh, G. Palazzo, G. Romanazzi, G. P. Suranna, N. Ditaranto, C. Di Franco, M. V. Santacroce, M. Y. Mulla, M. Magliulo and K. Manoli, *Faraday discussions*, 2014, **174**, 383.
25 K. Lee, J. H. Kim and S. Im, *Applied Physics Letters*, 2006, **88**, 023504.
26 D. De Tullio, M. Magliulo, G. Colafemmina, K. Manoli, L. Torsi and G. Palazzo, *Science of Advanced Materials*, 2013, **5**, 1922.
27 S. Zhang, N. Sun, X. He, X. Lu and X. Zhang, *Journal of physical and chemical reference data*, 2006, **35**, 1475-1517.
28 M. Moniruzzaman, N. Kamiya and M. Goto, *Organic & biomolecular chemistry*, 2010, **8**, 2887.
29 J. L. Kaar, A. M. Jesionowski, J. A. Berberich, R. Moulton and A. J. Russell, *Journal of the American Chemical Society*, 2003, **125**, 4125.
30 U. Kragl, M. Eckstein and N. Kaftzik, *Current Opinion in Biotechnology*, 2002, **13**, 565.
31 S. Y. Yang, F. Cicoira, R. Byrne, F. Benito-Lopez, D. Diamond, R. M. Owens and G. G. Malliaras, *Chemical Communications*, 2010, **46**, 7972.
32 S. M. Sze and K. K. Ng, *Physics of semiconductor devices*, John wiley & sons, 2006.
33 H. Yuan, H. Shimotani, J. Ye, S. Yoon, H. Aliah, A. Tsukazaki, M. Kawasaki and Y. Iwasa, *Journal of the American Chemical Society*, 2010, **132**, 18402.
34 V. Lockett, M. Horne, R. Sedev, T. Rodopoulos and J. Ralston, *Physical Chemistry Chemical Physics*, 2010, **12**, 12499.
35 G. Feng, R. Qiao, J. Huang, S. Dai, B. G. Sumpter and V. Meunier, *Physical Chemistry Chemical Physics*, 2011, **13**, 1152.
36 K. H. Lee, S. Zhang, T. P. Lodge and C. D. Frisbie, *The Journal of Physical Chemistry B*, 2011, **115**, 3315-3321.
37 J. Bisquert, G. Garcia-Belmonte, F. Fabregat-Santiago and P. R. Bueno, *Journal of Electroanalytical Chemistry*, 1999, **475**, 152.
38 A. E. S. A. http://www.abc.chemistry.bsu.by/vi/analyser/,
39 L. Kergoat, N. Battaglini, L. Miozzo, B. Piro, M.-C. Pham, A. Yassar and G. Horowitz, *Organic Electronics*, 2011, **12**, 1253.
40 P. R. Pudasaini, J. H. Noh, A. T. Wong, O. S. Ovchinnikova, A. V. Haglund, S. Dai, T. Z. Ward, D. Mandrus and P. D. Rack, *Advanced Functional Materials*, 2016.
41 M. Singh, M. Y. Mulla, M. V. Santacroce, M. Magliulo, C. Di Franco, K. Manoli, D. Altamura, C. Giannini, N. Cioffi and G. Palazzo, *Journal of Physics D: Applied Physics*, 2016, **49**, 275101.
42 I. Nausieda, K. K. Ryu, D. Da He, A. I. Akinwande, V. Bulovic and C. G. Sodini, *IEEE Transactions on Electron Devices*, 2010, **57**, 3027.
43 J. Hölzl and F. K. Schulte, in *Solid Surface Physics*, eds. J. Hölzl, F. K. Schulte and H. Wagner, Springer Berlin Heidelberg, Berlin, Heidelberg, 1979, 1.
44 J. Riviere, WORK FUNCTION--MEASUREMENTS AND RESULTS, 1969.
45 F. Silva, C. Gomes, M. Figueiredo, R. Costa, A. Martins and C. M. Pereira, *Journal of Electroanalytical Chemistry*, 2008, **622**, 153.
46 H. Liu, Y. Liu and J. Li, *Physical Chemistry Chemical Physics*, 2010, **12**, 1685.
47 U. Schröder, J. D. Wadhawan, R. G. Compton, F. Marken, P. A. Suarez, C. S. Consorti, R. F. de Souza and J. Dupont, *New Journal of Chemistry*, 2000, **24**, 1009.
48 J. G. Huddleston, A. E. Visser, W. M. Reichert, H. D. Willauer, G. A. Broker and R. D. Rogers, *Green chemistry*, 2001, **3**, 156.

Please do not adjust margins